Posters - Abstracts

# Localized hydrodynamics of clustering leucocytes

Adélia Sequeira, Abdel Monim Artoli

*Dept. of Mathematics and CEMAT / IST, Portugal.*
*{adelia.sequeira;artoli}@iseg.utl.pt*

Ana Santos Silva-Herdade, Carlota Saldanha

*Instituto de Biopatologia Química FML and Unidade de Biopatologia Vascular, IMM, Portugal.*
*anarmsilva@fm.ul.pt; Saldanha@medscape.com*

## Abstract

The recruitment of leukocytes to the endothelial walls is intensively investigated both experimentally and through three dimensional computer simulations. The shear dependent viscosity has been obtained from measured values in post-capillary venules of Whistar rats cremaster muscle. Localized velocity fields and shear stresses on the surface of leukocytes and near vessel wall attachment points have been computed and discussed for a cluster of recruited leukocytes under generalized Newtonian blood flow with shear-thinning viscosity. We have observed one region of maximum shear stress and two regions of minimum shear stress on the surface of the leukocytes close to the endothelial wall. This suggests that the accumulation of selectins attains a minimum value in two regions, rather than in one region, on the surface of the leukocytes. We have also verified that the collective hydrodynamic behavior of the cluster of recruited leukocytes establishes a strong motive for additional leukocyte recruitment. The study suggests that the influence of the leukocytes rolling on the increase of the endothelial wall shear stress may support the activation of more signalling mediators during inflammation [1,2,3].

# References

[1] A.M. Artoli, A. Sequeira, A.S. Silva and C. Saldanha, Leukocytes rolling and recruitment by endothelial cells: hemorheological experiments and numerical simulations, *Journal of Biomechanics*, in press.

[2] A.M. Artoli and A. Sequeira, Mesoscopic simulations of unsteady shear-thinning flows, *Computational Science* - ICCS 2006, series Springer Lecture Notes in Computer Science, vol. 3992, pp. 78-85, 2006.

[3] A.S. Silva, C. Saldanha, E. Martins, J. Silva, Effects of velnacrine maleate in the leukocyte-endothelial cell interactions in rat cremaster microcirculatory network. *Clinical Hemorheology and Microcirculation*, 36(3):235-46, 2007.

# Uncertainty Quantification with Polynomial Chaos Intrusive and non-Intrusive Approaches

Rita Ervilha

*Department o Mechanical Engineering, Instituto Superior Técnico, Thecnical University of Lisbon, Portugal.*
*rita.ervilha@gmail.com*

José Sereno

*Department o Mechanical Engineering, Instituto Superior Técnico, Thecnical University of Lisbon, Portugal.*
*rita.ervilha@gmail.com*

Miguel Abreu Almeida Mendes

*Department o Mechanical Engineering, Instituto Superior Técnico, Thecnical University of Lisbon, Portugal.*
*miguel.mendes@ist.utl.pt*

José Manuel Chaves Pereira

*Department o Mechanical Engineering, Instituto Superior Técnico, Thecnical University of Lisbon, Portugal.*
*jose.chaves@ist.utl.pt*

José Carlos Fernandes Pereira

*Department o Mechanical Engineering, Instituto Superior Técnico, Thecnical University of Lisbon, Portugal.*
*jcfpereira@ist.utl.pt*

## Abstract

The uncertainty is a permanent reality everytime one wants to understand or characterize some physical aspect. In the present work we intent to present and analyse the uncertainty quantification in several cases and with the recourse to different techniques.

Being that Monte-Carlo methods are very expensive and time consuming, namely for a high level of confidence, we use the Polynomial Chaos expansions to simulate the uncertainty propagation along the time and the physical space. Analytical and numerical projections of the stochastic equations into an orthogonal basis of the polynomials are computed leading to different kinds of methods, the intrusive and non-intrusive methods, respectively.

Several cases concerning the different approaches are presented and some numerical and physical aspects analysed. Also, both Hermite and Laguerre polynomials are considered, associated to the Normal and Gamma probability density functions.

Particularly, we have considered three different cases: - Time and space evolution of a 2D Lamb-Oseen vortice and a pair of vortices in cross flow where the viscosity is

a random input as a way of simulate a range of Reynolds numbers. - One-Dimensional reacting flows inside porous burners with stochastic physical parameters as the convection coefficient or the medium porosity is one example of dealing with properties which can substancialy vary from each manufacturer. - Propagation of forest fires with the classical Rothermel method affected by uncertainty in several input variables. This type of physical modelling is one of the most affected by the uncertainty in the relevant parameters. Here, the moisture and wind direction and intensity are some of the stochastic variables that must be considered.

# A non Linear PDE in image's restoration

R. Aboulaich[1], S. Boujena[2] and E. El Guarmah[1]

[1] *LERMA, Mohammadia Engineering School, Mohamed V University, Ibn Sina Str., POB 765 Agdal, Rabat, Morocco*
*aboulaich@emi.ac.ma*
*guarmah@gmail.com*

[2] *Département de Mathématiques et Informatique, Faculté des Sciences Ain Chock, Km8 Route El Jadida, BP 5366 Maârif, Casablanca*
*boujena@yahoo.fr, s.boujena@fsac.ac.ma*

## Abstract

In this paper, we present a nonlinear parabolic model for image processing. The existence, the uniqueness and stability of the solution are obtained. Using a finite difference method we experiment the validity of the proposed model and we illustrate the efficiency of the method.

**Keywords:** Image restoration, Nonlinear parabolic model, Hilbert space.

## 1 Introduction

In this paper we are interested to restore the noisy image $u_0$ by a PDE problem

$$\begin{cases} \dfrac{\partial u}{\partial t} - \operatorname{div}[\mu(\mid \nabla u \mid)\nabla u] = 0 \ in \ Q \\ u(x,t) = 0 \qquad \forall x \in \partial\Omega \qquad \forall t \in [0,T], \\ u(x,0) = u_0 \qquad \forall x \in \Omega. \end{cases} \tag{1}$$

Where $\Omega$ is an open bounded subset of $\mathbb{R}^N$, $N = 2$ or $N = 3$, with boundary $\partial\Omega$, $Q = \Omega \mathrm{x}[0,T]$ with some given $T > 0$ and $\mu$ verifies the following hypothesis:

(1.1) $\mu : \mathbb{R}_+ \to \mathbb{R}_+$     (1.2) $\mu$ is continuous function     (1.3) $\lim\limits_{s \to +\infty}[\mu(s)] = \mu_0$ with $\mu_0 > 0$

    (1.4) $\mu$ is differential continuous         (1.5) $s \mid \mu'(s) \mid \le \mu(s) \ \forall s \in \mathbb{R}_+$

The existence and the uniqueness of a solution of the used non linear PDE problems are in general difficult to establish, an approch using the Galerkin method is proposed in several works, see [4], for solving the existence solution in Hilbert spaces. Many algorithms are proposed for image processing, see [2, 3]. In the case of this work the non linear PDE problem has an unique solution in a Hilbert space and we have good numerical results, see [1].

**Theorem 1.1 (Stability theorem)** *Let $\mu_1$ and $\mu_2$ verifie* $(1.1) - (1.5)$. *It is assumed more that* $\inf\limits_{s \in \mathbb{R}_+} \mu_1(s) = b_1 \ne 0$ *or* $\inf\limits_{s \in \mathbb{R}_+} \mu_2(s) = b_2 \ne 0$ *Then there exists a constant* $K > 0$ *such that* $\mid u_1 - u_2 \mid_{L^\infty(0,T,H)} \le K \sup\limits_{s \in \mathbb{R}_+} \mid \mu_1(s) - \mu_2(s) \mid$ *with* $K = \dfrac{1}{\sqrt{b_2}}\|u_1\|_{L^2(0,T,V)}$ *or* $K = \dfrac{1}{\sqrt{b_1}}\|u_2\|_{L^2(0,T,V)}$

Where $V = H_0^1(\Omega)$ is the adherence of $\mathcal{D}(\Omega)$ in $H^1(\Omega)$.

For the numerical experiments we consider the following model:

$$\begin{cases} \dfrac{\partial u}{\partial t} - div\Big(\big(\dfrac{1}{\sqrt{1 + (\mid \nabla u \mid)^2}} + \alpha\big)\nabla u\Big) = 0 & in\ Q \\ u(x,0) = u_0 & in\ \Omega, \qquad u(x,t) = 0\ \forall\ x \in \partial\Omega\mathrm{x}[0,T]. \end{cases} \tag{2}$$

where $u$ represents the processed image. Equation (2) is discretized using the finite difference method. We use an explicit scheme which gives a correct solution when the coefficient $\alpha$ is too low. Note that the boundary conditions $u = u0$ on $\partial\Omega\mathrm{x}[0,T]$ of the problem (1) is tested numerically for restored image but its mathematical study is underway realized, see Figure 1.
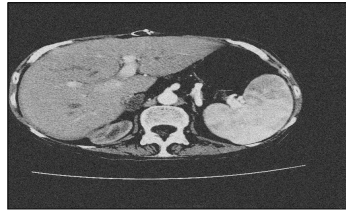


Image original (a)          Noisy Image (Gaussian 15%)



Restored Image with $u = 0$ on $\partial\Omega\mathrm{x}[0,T]$     Restored Image with $u = u_0$ on $\partial\Omega\mathrm{x}[0,T]$

**Figure 1.** The Restored image with $\alpha = 10^{-6}$

# 2  Conclusion

We proposed in this work a nonlinear parabolic PDE model for the medical image processing. After the mathematical analysis of the PDE problem, we tested the model numerically. The obtained results show the effectiveness of the approach.

**References**

[1] R. Aboulaich , S. Boujena and E. El Guarmah, *Sur un modèle non-linéaire pour le débruitage de l'image*, C. R. Acad. Sci. Paris, Ser. I 345, pp. 425-429, 2007.

[2] L. Alvarez, P-L. Lions and J-M. Morel, *Image selective smoothing and edge detection by nonlinear diffusion. ii*, SIAM Journal on Numerical Analysis, 29 (3), pp. 845-866, 1992.

[3] G. Aubert and P. Kornprobst, *Mathematical problems in image processing*, Springer-Verlag, New-York, 2002

[4] S. Boujena, *Etude d'une classe de fluides non newtoniens, les fluides newtoniens généralisés*, thèse de 3ème cycle, Université Pierre et Marie Curie -Paris 6, 1986.

# Advances in Computational Hemorheology

João P. Janela

*Dept. of Mathematics ISEG and CEMAT / IST, Portugal.*

*jjanela@iseg.utl.pt*

Adélia Sequeira, Abdel Monim Artoli, Euripides Sellountos

*Dept. of Mathematics and CEMAT / IST, Portugal.*

*{adelia.sequeira; artoli; esell@math.ist.utl.pt*

## Abstract

Experimental investigations conducted over the years have shown that blood can exhibit non- Newtonian characteristics like shear-thinning, viscoelasticity and thixotropy. The ability to describe the complex rheological behaviour of blood, which is determined by numerous physiological factors like plasma viscosity, rate of shear, haematocrit or level of red blood cell aggregation and deformability, among others, is of major importance in many clinical applications, where local hemodynamics plays a determinant role. A detailed discussion of different models and methods can be found in [4].

In some districts of the vascular system, like in large vessels, blood viscosity can be considered as a constant and blood flow is well described by the Navier-Stokes equations. In smaller vessels, the non-Newtonian effects are not negligible and more complex models must be used. A constitutive law, involving a nonlinear relation between the stress and the deformation gradient, is added to the system of equations.

The mathematical and numerical analysis of these complex problems can become a formidable task, both from the theoretical and the computational view points. In our presentation we show some results of blood flow simulations, using different numerical techniques, to study hemodynamical and hemorheological circulation effects [1, 2, 3, 5].

# References

[1] A. M. Artoli, J. Janela and A. Sequeira, The role of Womersley number in shear-thinning fluids, *Transactions on Fluid Mechanics*, Issue 2, Vol. 1, pp 133-139, 2006.

[2] A.M. Artoli, A. Sequeira and J.P. Janela, Shear-thinning viscosity effects in bifurcating blood vessels, *Journal of Biomechanics*, Volume 39, Supplement 1, 2006, Page S310.

[3] J. Janela and A. Sequeira, On a constrained optimization problem arising in Hemodynamics, *Banach Center Publications*, Vol 80, 2008.

[4] A. Sequeira and J. Janela, An overview of some mathematical models of blood rheology, in: *A Portrait of State-of-the-Art Research in the Technical University of Lisbon* (M.S. Pereira Ed.), Springer, 2007.

[5] E. Sellountos and A. Sequeira, An advanced meshless LBIE/RBF method for solving two dimensional incompressible fluid flows, *Computational Mechanics*, to appear.

# Three-Dimensional Reconstruction of Biomechanical Structures for Finite Element Analysis

D.S. Lopes, J.A.C. Martins, E.B. Pires

*DECivil and ICIST, Instituto Superior Técnico, Technical University of Lisbon, Portugal.*
*{danlopes, jmartins, bpires}@civil.ist.utl.pt*

## Abstract

Medical imaging modalities, such as computed tomography (CT) and magnetic resonance (MR), provide 3D anatomophysiological data that allow clinicians and surgeons to carry out important medical decisions. For the biomechanical engineering community, medical images are perceived as the input signal for a geometric modeling pipeline that outputs accurate 3D CAD and mesh models. These models are extensively used for finite element (FE) analysis in order to study several biomedical phenomena. Our framework for 3D anatomical modeling starts by filtering image data to reduce noise and artifacts: an anisotropic diffusion filter plays here an essential role. The structures of interest are then partitioned into voxelized images, using, for instance, a 3D snake segmentation algorithm with a contour evolution equation solved by a level set method. To convert this type of image data into surface data, mesh-based or CAD-based geometric modeling reconstruction approaches may be adopted. The most usual mesh-based techniques rely on extracting a polygonal isosurface by the marching cubes algorithm. The isosurface needs then to be smoothed and decimated, so that unwanted features are removed. CAD-based methods rely on point cloud extraction with further cubic spline curve or surface patch interpolation. In this manner a mathematical representation of the anatomical geometry, or solid model, is created. And, whenever a volumetric analysis is required, tetrahedral or hexahedral meshes can be generated from an isosurface or a CAD model. The 3D models created by either modeling approach can also be utilized for medical visualization and rapid prototyping purposes. Several finite element models developed at ICIST–IST are presented (cf. Figure 1) together with the sequence of image processing and geometric modeling techniques applied in each case: the pelvic floor muscles [1], the thoracic diaphragma, the long bones of the upper and lower limbs [2], a bovine calf femur diaphysis [3], the femuroacetabular articulation. A vast range of software tools were used for modeling the geometry of these biomechanical structures, namely: MATLAB, ITK–SNAP, ParaView, Blender 3D, Rhinoceros, CUBIT, ABAQUS.

**Keywords:** Medical Image, Isosurface, Solid Model, Computer-Aided Design, Finite Element Analysis, Biomechanics.
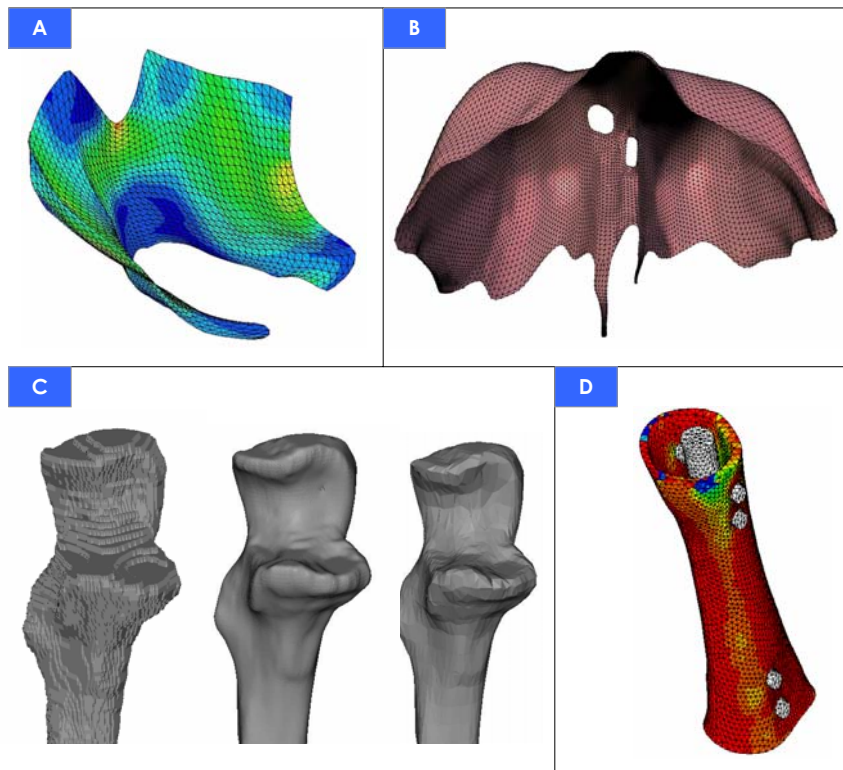
Figure 1: FE models developed at ICIST: A) female pelvic floor; B) thoracic diaphragm; C) isosurface, smoothed and decimated meshes of ulna's proximal epiphysis; D) bovine femur diaphysis with interlocking nail.

# References

[1] JAC Martins, M Pato, EB Pires, RMN Jorge, M Parente, and T Mascarenhas, Finite Element Studies of the Deformation of the Pelvic Floor, *Annals of the New York Academy of Sciences*, 11(01), 2007.

[2] DS Lopes, JAC Martins, JG Campos, and EB Pires, Modelação Geométrica de Estruturas Humanas Baseada em Imagens de Tomografia Computarizada, *CMNE/CILAMCE*, 2007.

[3] DS Lopes, LB Rodrigues, EB Pires, JAC Martins, EB Las Casas, RR Faleiros, J Folgado, and PR Fernandes, Development of solid and finite element models of bovine bone for veterinary research, *CONEM*, 2008.

# An anisotropic error indicator for Finite-Volume methods

João Paulo Magalhães
*jpmagalhaes@ist.utl.pt*

José Manuel Chaves Pereira
*jose.chaves@ist.utl.pt*

José Carlos Pereira
*jcfpereira@ist.utl.pt*

*LASEF – Laboratory and Simulation in Energy and Fluids*
*Departamento de Engenharia Mecânica*
*Instituto Superior Técnico*
*Av. Rovisco Pais 1049-001 Lisboa, Portugal*
*web page: http://www.lasef.ist.utl.pt*

### Abstract

The refinement criterion used in adaptive Finite Volume methods has not been subject to as much attention as in Finite Element methods, mainly because theoretical treatment and error analysis place more difficulties. In this communication, we propose a statistical approach to obtain a local anisotropic error indicator suitable for use in Finite Volume methods. By performing a specification analysis on the order of the Taylor Series for the local profiles, we obtain an error indicator which detects simultaneously large-scale and small-scale flow phenomena. A 1D analysis is performed, and results are presented for the the analytical and lid-driven cavity flow.

**Keywords:** $h$-refinement, anisotropic, error estimation, regression diagnostics

# Flame Stability Analysis in Inert Porous Burners

Miguel Abreu Almeida Mendes

*Department o Mechanical Engineering, Instituto Superior Técnico, Thecnical University of Lisbon, Portugal.*
*miguel.mendes@ist.utl.pt*

José Manuel Chaves Pereira

*Department o Mechanical Engineering, Instituto Superior Técnico, Thecnical University of Lisbon, Portugal.*
*jose.chaves@ist.utl.pt*

José Carlos Fernandes Pereira

*Department o Mechanical Engineering, Instituto Superior Técnico, Thecnical University of Lisbon, Portugal.*
*jcfpereira@ist.utl.pt*

## Abstract

This work presents a numerical study of the stabilisation diagram of premixed flames in a finite porous media inert ceramic foam. A set of steady computations are considered, using a 1D numerical model which takes into account solid and gas energy equations as well as chemistry and radiation models. The present results show that both stable and unstable solutions, for upper and lower flames, exist either at the surface or submerged in the porous matrix.

A linearised version of Discrete-Ordinates radiation model is included in the linear stability analysis to discuss the influence of radiation in the stability of the flames. The full stabilisation diagram and the linear stability analysis provide information on the stability of the flames, pointing to the existence of surface and submerged flames that can be unstable. The analysis of the slope of the power as well as the eventual existence of flashback windows can help us to understand not only the locus of the real flames but also its behaviour in some situations.

The stability analysis was done to premixed methane/air flames and ultra-lean $H_2$/CO mixtures, and a simplified reaction kinetics (2-step mechanism) was employed in order to perform a linear stability analysis. This results are used to investigate the stability of the steady solutions as a function of burning velocity and flame location for a set of different inlet conditions.

From the linear stability results it can be concluded that the insertion of inert porous media for premixed combustion promotes the stability of the analysed flames.

**Keywords:** Premixed combustion, Inert porous media, Linear stability analysis, Radiation, Flame stabilisation.

# Numerical simulation of in-vitro dispersion and deposition of nanoparticles in dry-powder-inhaler aerosols

P. J. Mendes[a,b], J. F. Pinto[b] and J. M. M. Sousa[a]

*a - IDMEC/IST, Mecânica I, 1º andar/LASEF,*
*Av. Rovisco Pais, 1049-001 Lisbon,*
*PORTUGAL.*
*b - Dept. de Tecnologia Farmacêutica,*
*Faculdade de Farmácia da Universidade de Lisboa,*
*Av. Prof. Gama Pinto, 1649-003 Lisboa,*
*PORTUGAL.*
*msousa@ist.utl.pt*

## Abstract

Aerosol dispersion and deposition inside an idealized mouth-throat has been numerically simulated using a stochastic Lagrangian model accounting for Brownian motion and particle-wall interaction. Delivery of nanoparticles to the lungs is extremely difficult, mainly due to their low inertia, and for this reason they are often loaded into larger carrier particles. Bearing in mind the potentialities of nanoparticles in advanced drug delivery, a set of monodisperse particles with diameters in the nanosize range, as well as in the respirable and carrier ranges, were considered in the present simulations. Deposition patterns were obtained by tracking a total of 16,000 particles for each diameter. The results have shown that similar patterns were obtained in the mouth-throat for 400 nm particles and larger. A clear correspondence between secondary flow structures in the fluid and these deposition patterns was observed, demonstrating the role of the convective transport processes for this size range. In contrast, a much more uniform distribution of the particles adhering to the walls was noted for a size of 200 nm. It was also found that a very large amount of these particles (nearly 80%) is lost by deposition on the mouth-throat, thus recommending the use of (larger) carrier particles.

# Coupling multiscale fluid-structure interaction models for blood flow simulations

Alexandra B. Moura

*CEMAT, Center for Mathematics and its Applications, Department of Mathematics, IST, Lisbon, Portugal.*
*alexandra.moura@math.ist.utl.pt*

## Abstract

Over the last years, mathematical modelling and numerical simulations of blood flow have gained a great relevance in the understanding of the human cardiovascular system, in particular the origin and development of cardiovascular diseases [1]. However, modelling the human circulatory system remains a very difficult and challenging task because of its complexity and heterogeneity, both geometrically and functionally. In particular, realistic numerical simulations of blood flow in arteries can not be performed without taking into consideration the link between local and global phenomena [1, 2]. Moreover, blood flow is characterized by pulse waves due to the fluid-structure interaction (FSI) between blood and the vessel wall, which should be properly captured by the numerical model [2, 3].

The geometrical multiscale modelling of the cardiovascular system was introduced to deal with this complexity and diversity. It consists of a hierarchical description, in which the different parts of the circulatory tree are approximated at different dimensional scales, 3D, 1D and 0D, corresponding to different levels of desired accuracy [2]. At the higher level are the three-dimensional (3D) models. They describe very accurately the blood flow velocity and pressure fields, but in practice they are applied only to relatively small computational domains. This fact is linked to their computational cost, the impossibility (at least for now) of representing the whole 3D geometry of the circulatory system, and the fact that detailed information is usually needed only in specific regions of interest, such as bifurcations or stenosed vessels. On the artificial sections generated by the 3D domain truncation, one can account for the remaining parts of the cardiovascular system by using measured data or by means of simpler, reduced one-dimensional (1D) or lumped parameter (also called 0D) models. They are usually obtained by making simplifying assumptions and performing averaging procedures on the 3D model. In particular, the 1D models are described by hyperbolic systems of PDEs and, despite having a lower level of accuracy compared to the full 3D model, are still able to capture effectively the pulse waves characteristic of blood flow. Coupled to the 3D detailed problem, the 1D models can act as absorbing (or far field) boundary conditions. Moreover, due to their low computational cost, they can be used to simulate large parts of the arterial tree.

One of the challenging tasks in using the geometrical multiscale approach is the setting of proper coupling conditions to exchange quantities such as the flow rate or the mean pressure at the interfaces between different models. When using compliant geometries for the 3D simulation there is the additional request of having an appropriate condition for the arterial wall deformation at the interface [2, 3].

In this study we focus on the coupling between the three different types of models, with particular emphasis on the coupling between 3D and 1D models [2, 3]. The 3D model consists of the Navier-Stokes equations for incompressible and Newtonian fluids, since we apply it in medium to large vessels where blood is assumed to be Newtonian, coupled with a model for the vessel wall. We discuss different strategies to impose the continuity of the flow rate, mean pressure and area at the interface between the 3D and 1D models. Furthermore, we consider an anatomically 3D realistic compliant model of a human carotid bifurcation coupled with reduced models at the downstream sections, including a 1D network representation of the circle of Willis [2, 4].

**Keywords:** mathmatical models, numerical simulations, geometrical multiscale approach, fluid-structure interaction (FSI), 3D FSI - 1D coupling.

# References

[1] L. Formaggia, A. Quarteroni and A. Veneziani, *The circulatory system: from case studies to mathematical modelling*, in: Complex Systems in Biomedicine, A. Quarteroni, L. Formaggia and A. Veneziani editors, 243-287, 2006, Springer Milan.

[2] A. Moura, *The geometrical multiscale modeling of the cardiovascular system: coupling 3D FSI and 1D models*, PhD thesis, Politecnico di Milano, May 2007.

[3] L. Formaggia, A. Moura and F. Nobile. *On the stability of the coupling of 3D and 1D fluid-structure interaction models for blood flow simulations.* ESAIM: Mathematical Modelling and Numerical Analysis (M2AN), 41(4):743-769, 2007.

[4] A. Moura, M. Prosi, F. Nobile and L. Formaggia, *Absorbing boundary conditions for pulse propagation in arteries, Journal of Biomechanicsecture*, Volume 39, Suplement 1, 2006, Page S440.

# Simulation of turbulent accelerated jets for aeronautical applications

Pedro Neto

*LASEF / IDMEC, Instituto Superior Técnico, Portugal.*

*pmrfn@clix.pt*

Carlos B. da Silva

*LASEF / IDMEC, Instituto Superior Técnico, Portugal.*

*carlos.silva@ist.utl.pt*

José C. F. Pereira

*LASEF / IDMEC, Instituto Superior Técnico, Portugal.*

*jcfpereira@ist.utl.pt*

## Abstract

Several direct and large-eddy simulations (DNS & LES) are performed using a previously validated pseudo-spectral code [1] to analyze the kinematics and topology of the primary coherent structures and the entrainment rate during acceleration. The Reynolds number ranges from $Re_D = 5 \times 10^2$ to $Re_D = 2 \times 10^4$ and the constant acceleration rate ranges from $\alpha = 0.04$ to $\alpha = 0.06$. Figures 1 and 2 show results for Q criteria and an acceleration map which along with spectra of various quantities are used to study the kinematics [2] and topology of the three-dimensional coherent structures confirming that these are quite different during the acceleration phase as the Kelvin-Helmholtz vortex rings are much smaller and more stable. These also show an higher shedding frequency as shown in Figure 3. Contrary to previous ideas [3] [4], the jet's entrainment rate is higher during the acceleration phase, even though the jet spreading rate is reduced.

**Keywords:** DNS, LES, unsteady, turbulent, jet, coherent, structures, entrainment.

# References

[1] DA SILVA, C. B. & MÉTAIS, O. 2002 Vortex control of bifurcating jets: a numerical study *Phy. Fluids* **14**. 3798–3819.

[2] ZHANG, Z. & JOHARI, H. 1996 Effects of acceleration on turbulent jets *Phy. Fluids* **8**, 2185–2195.

[3] KOUROS, H., MEDINA, R. & JOHARI, H. 1993 Spreading rate of an unsteady turbulent jet *AIAA Journal* **29**, 1524–1526.

[4] KATO, S., GROENEWEGEN, B. & BREIDENTHAL, R. 1986 Turbulent mixing in nonsteady jets *AIAA Journal* **25**, 165–167.
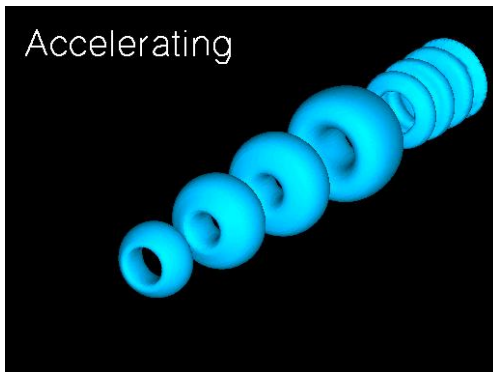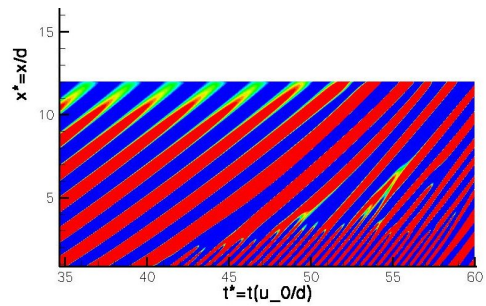
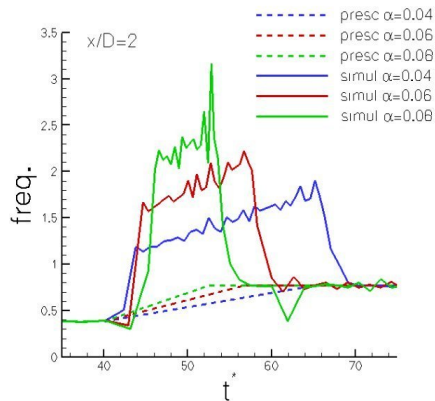Figure 1 - Q Isosurfaces



Figure 2 - Acceleration Map



Figure 3 - Kelvin-Helmholtz frequency

# Comparison between two 1D models for blood flow in arteries

Diana Nunes

*Department of Physics, IST, Lisbon, Portugal*
*di_catarina@msn.com*

Susana Ramalho

*Department of Physics, IST, Lisbon, Portugal*
*nana_ramalho@hotmail.com*

Alexandra Moura

*CEMAT, Department of Mathematics, IST, Lisbon, Portugal*
*alexandra.moura@math.ist.utl.pt*

Adélia Sequeira

*CEMAT, Department of Mathematics, IST, Lisbon, Portugal*
*adelia.sequeria@math.ist.utl.pt*

## Abstract

Every year millions of people die due to cardiovascular diseases, which are one of the main causes of death in industrialized countries. The study of blood flow dynamics through mathematical models and numerical simulations constitutes an important, non invasive, tool to help the prediction of pathologies, as well as the consequences of surgery. In particular, the application of mathematical simplified models have proved to give useful information at a fair computational cost [1, 2].

In this work two types of reduced one-dimensional (1D) models for blood flow in arteries are studied. The 1D models describe the evolution in time and one dimensional space coordinate, of the mean pressure, flow rate and area. These models describe very well the wave pressure propagation, which is a characteristic of blood flow in arteries.

First we consider a purely 1D hyperbolic model [3]. This model has already been used in several applications [1, 2]. Each vessel of the arterial network is described by a one dimensional system of two partial differential equations plus a closing pressure-area algebraic relation. Considering each artery as a straight cylinder, the basic nonlinear hyperbolic model is derived assuming axial symmetry, radial displacements, fixed cylinder axis, constant pressure on each axial section, no body forces and dominance of axial

velocity [3]. The system is discretized using a second order Taylor-Galerkin scheme and the Lax-Wendroff scheme[3].

Afterwards we take an hybrid 1D model, where the arterial pressure and flux are separated into wave and reservoir components [4, 5]. The time-varying reservoir component is described by a Windkessel model [4, 5] and the wave component is described by the 1D hyperbolic model mentioned above. This way, the pressure at the beginning of systole is given by the reservoir pressure. The model is derived assuming that the pressure fall-off in diastole is fitted to an exponential function and that the flow and the wave pressure, as well as the local reservoir velocity and reservoir pressure, are proportional.

The pressure and flux distributions of both models in the considered vessel are compared also using patterns reported in literature. Properties and strengths of the models, regarding the numerical simulations in view of clinical applications are analyzed and their limitations and drawbacks commented.

**Keywords:** 1D models, artery, blood flow, wave pressure, hyperbolic model, Windkessel model.

# References

[1] J. Alastruey, K.H. Parker, S.M. Byrd, J. Peiro, S.J. Sherwin, *Modelling the circle of Willis to assess the effects of anatomical variations and occlusions on cerebral flows.* Journal of Biomechanics, 40(8), pp. 1794-1805, 2007.

[2] V.E. Franke and K.H. Parker and L.Y. Wee and N.M. Fisk and S.J. Sherwin, *Time domain computational modelling of 1D arterial networks in monochorionic placentas.* Mathematical Modelling and Numerical Analysis (M2AN), 37, pp. 557-580, 2003.

[3] Formaggia and A. Veneziani. *Reduced and multiscaled models for the human cardiovascular system.* Lecture notes VKI Lecture Series 2003-7, Brussels, 2003.

[4] J. E. Davies, N. Hadjiloizou, D. Leibovich, A. Malaweera, J. Alastruey-Arimon, Z. I. Whinnett, C. H. Manisty, D. P. Francis, J. Aguado-Sierra, R. A. Foale, I. S. Malik, K. H. Parker, J. Mayet and A. D. Hughes. *Importance of the aortic reservoir in determining the shape of the arterial pressure waveform. The forgotten lessons of Frank.* Artery Research. Volume 1, Issue 2, September 2007, pp. 40-45.

[5] Jazmin Aguado-Sierra, *Application of wave intensity analysis in the cardiovascular system.* Ph.D. Thesis, Department of Bioengineering, Physiological Flow Studies Group ,Imperial College London, 2007.

# Simulation of Dragonfly Hovering Under Ground Effect

José Manuel Chaves Pereira

*Department o Mechanical Engineering, Instituto Superior Técnico, Thecnical University of Lisbon, Portugal.*
*jose.chaves@ist.utl.pt*

José Carlos Fernandes Pereira

*Department o Mechanical Engineering, Instituto Superior Técnico, Thecnical University of Lisbon, Portugal.*
*jcfpereira@ist.utl.pt*

## Abstract

Recently, interest has been growing in studying insect flight and applying its knowledge to the development of micro air vehicles (MAV) that could be used for surveillance or search and rescue. Some authors indicated that insect flight could be a very successful design for MAVs because they have much better aerodynamic performance than conventional wings and rotors.

To study the unsteady flows and forces on flapping wings at Reynolds number in between 10 to $10^4$, biologists developed experiments of mechanic wings scaled up from a hawkmoth and a fruit fly. In parallel, computer codes were developed to solve the Navier-Stokes equation around a moving wing. Several three dimensional numerical techniques have been applied to insect flight, however a two-dimensional (2D) slice of the problem is relevant to study the basic mechanisms in flapping flight before the detailed three dimensional calculations that require huge computing requirements.

Insect flight performance depends on the way that the wing interacts with its wake and with the shed vortices. This fact is even more relevant during hovering, as the wing-wake interaction is even more emphasized. The complex interaction between the wing and its wake is an aerodynamic characteristic of the insect flapping flight and any successful aerodynamic model must be able to capture these complex interactions. The CFD software Star-CD was selected and forward flapping flight and ragonfly and hovering will be predicted to validate the present predictions of the flapping flight. To the authors knowledge, the dragonfly hovering flapping wing aerodynamics was only considered in free flight without the ground effect. Insects do all flight modes near the ground and MAVs are expected to do so. The main objective of the present study is to predict the flapping dragonfly hovering characteristics under ground effect.

**Keywords:** Flapping flight , Hovering, MAV, insect flight.

# Simulation and Analysis of the Flow Inside SiSic Porous Foams

José Manuel Chaves Pereira

*Department o Mechanical Engineering, Instituto Superior Técnico, Thecnical University of Lisbon, Portugal.*
*jose.chaves@ist.utl.pt*

José Carlos Fernandes Pereira

*Department o Mechanical Engineering, Instituto Superior Técnico, Thecnical University of Lisbon, Portugal.*
*jcfpereira@ist.utl.pt*

## Abstract

The flow in porous media have been an intensively explored field since Henry Darcy in the nineteenth century From the reservoir rocks, petroleum engineering, geology, to porous membranes or combustion in porous foams, a lot of work have been developed. However most of the numerical simulations concerning the real flow in porous media was related to packed bed of spheres. In the present work we simulate and analyse the flow inside SiSic Porous foams.

The SiSic porous foams is one of the porous materials used to fill combusters so that burners can be more compact and the combustion more complete and with less polutants. This, among other applications.

With the increase of resolution and easiest acess to comercial facilities of CAT, it is now feasible to get the real computational geometry of porous media.

Starting from a 3D CAT scan of a SiSic foam, and after due geometrical treatments, we replicate the sample in order to get a desired geometry. Note that, even in the real applications, most of times the porous blocks are made from slides joined together. From the computational model of the porous foam, the generation of a fluid space grid was the next step.

The numerical simulations was done for pore Reynolds numbers ranging from 1 to 2000 to characterize the influence of the Reynolds in the flow field and different geometries was also taken into acount.

In this work we fully characterize the flow inside the foam in terms of the relevant parameters. The pressure drop, the residence time, the normal and viscous forces as well as the pdf's of the velocity field and energy are some of the physical parameters taken into acount in this study.

**Keywords:** SiSic Foams, Flow in porous media, Pressure drop.

# THE IMPACT OF UNCERTAINTY IN MEDICAL IMAGE SEGMENTATION ON VASCULAR DISEASE

Angela M.M.O. Pisco*

*MEBM,Departamento de Física, Instituto Superior Técnico, Portugal.*
*angela.oliveira.pisco@ist.utl.pt*

Nuno J. G. Santos*

*MEBM,Departamento de Física, Instituto Superior Técnico, Portugal.*
*nuno.dodgeps@gmail.com*

Alberto M. Gambaruto

*CEMAT,Departamento de Matemática, Instituto Superior Técnico, Portugal.*
*alberto.gambaruto@yahoo.com*

Adélia Sequeira

*CEMAT,Departamento de Matemática, Instituto Superior Técnico, Portugal.*
*adelia.sequeira@math.ist.utl.pt*

*\* Both authors contributed equally for present work*

## Abstract

Medical image segmentation has been extensively explored in recent years, but the interlaced dependence on the resulting fluid dynamics still needs to be explored. In imaging processing, it is important to select an adequate threshold for extracting desired objects from their background, and in our case we require to extract the arterial lumen. Several thresholding techniques have been evaluated in [2], for images containing text or shapes, with the conclusion that clustering methods yield consistently superior results. No conclusive studies of medical image segmentation exist, that relate the different reconstructed virtual models with the resulting flow field, indicating the extent of the variations from a physiological viewpoint.

Arterial fluid dynamics depends on the conduit geometry [1], furthermore it is also postulated that the locations of atheroma in coronary arteries are linked to regions of low wall shear stress and flow recirculation in steady flow [1]. In this study we use a stack of medical images obtained from magnetic resonance imaging (MRI), from a planar, small graft-proximal angle (GPA) anastomosis, located on the popliteal artery, below the knee [1, 3]. Four different techniques for image segmentation were used in order to reconstruct a virtual model for fluid dynamic numerical simulations. The aim is to devise measures that characterize morphological variations and the corresponding changes in flow field.

The clustering methods used are automatic and iterative: Kittler [4], Otsu [5], Ridler [6] and Local Mean (LM). Figure 1 shows the variation of the threshold values along the stack of cropped medical images, for the each of the proposed methods.
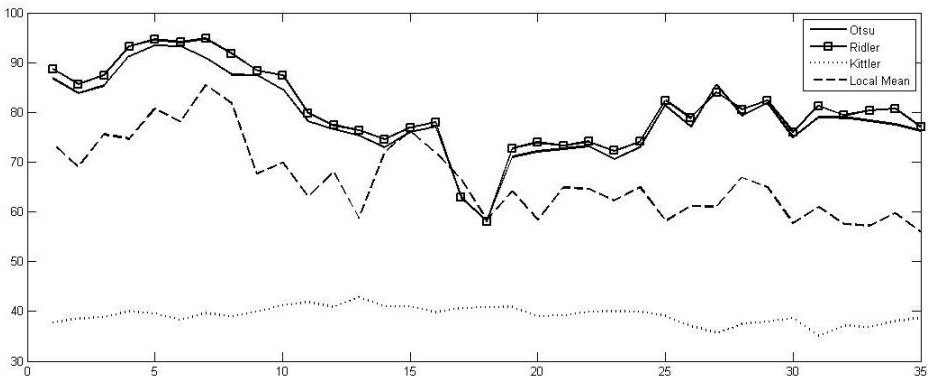


Figure 1: Threshold variation along the stack of cropped medical images.

The Kittler method, found in [2] to yield consistent superior results, considers thresholding as a classification problem of the background and object, and is based on fitting Gaussian distributions to the histogram of the grey scale values of the image pixels. The Otsu method also uses the histogram distribution of the grey scale values, once again dividing the image into background and object, however the approach here is to maximise the standard deviation of the grey scale of each region. The Ridler method works once again by dividing the image into background and object, associating to each an average grey scale value, with the delineating threshold given as the mean of the background and object grey scale values.

The LM method is a novel approach, based on the Ridler idea. In this technique, each image is again divided into two classes, the background and the object, however the mean threshold value associated with each of these classes is now found locally, at the region of interface between the two classes. The main advantage is that the segmentation is based on local information and not global as in [6], hence the sensitivity increases as can be seen in the reconstructions and threshold value selection. Increased sensitivity however implicates a greater influence from noise.

All images are cropped around the region of interest. This is done to reduce the effect of noise and increase the sensitivity of the methods. The scale space filter [7] is then also used to reduce the effect of noise on the image segmentation.

A three dimensional surface definition is obtained interpolating the segmented stack of closed contours using implicit functions with cubic radial basis functions (RBF) inter-

polation [8], that minimizes the curvature of the function. Given the size of the data set to reconstruct, the partition of unity approach [9] is used to resolve the linear system. Furthermore, the desired iso-surface that defines the geometry is triangulated using the marching tetrahedra method [10]. This is all performed using in-house codes.



Figure 2: Geometry reconstruction after segmentation with Ridler method.

Morphological comparison of the reconstructed geometries using the four segmentation methods is performed by observing where the greatest difference in the surface definition occurs. This is obtained in a variety of measures, including: the closest distance between the different surface definitions, the volumes, surface areas, amongst others.

Numerical simulations of the fluid dynamics are performed using the commercial software Fluent. The mean velocity was measured using Doppler ultrasound *in vivo*. Blood was assumed to be an incompressible Newtonian fluid. The Reynolds number based on the bypass conduit inflow diameter was found to be $Re =135$, low enough for the flow to be considered laminar, with a 40% proximal and 60% distal outflow split. The flow was considered steady and a Poiseuille flow velocity profile was used at the inflow. The mesh contains approximately 1.5 million cells, with a fine near wall region of wedge shaped elements and a unstructured tetrahedral core [3].

To compare the flow field of the different virtual models, the wall shear stress is used as the key parameter, given its postulated link to atherosclerosis.
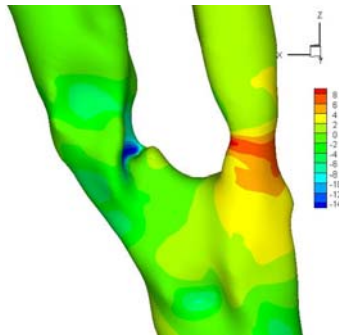
Figure 3: Wall shear stress distribution in the anastomosis virtual model, segmented using the Ridler method.

We report that using different methods of medical image segmentation can yield noticeably altered wall shear stress distributions, which can lead to varied interpretation of the healthcare of the subject. This study identifies a research topic that has a high impact in the field of patient-specific studies performed from medical images; indicating a need to obtain more robust methods of medical image segmentation and a measure of uncertainty associated to the results obtained for patient-specific studies.

**Keywords:** *medical image segmentation comparison, arterial fluid dynamics, uncertainty estimation.*

# References

[1] S. Giordana, S. J. Sherwin, J. Peiró, D. J. Doorly, J. S. Crane, K. E. Lee, N. J. W. Cheshire and C. G. Caro, "Local and Global Geometric Influence on Steady Flow in Distal Anastomoses of Peripheral Bypass Grafts",*Journal of Biomechanical Engineering*, **127**, pp. 1087-1098, December 2005

[2] Mehmet Sezgin and Bülent Sankur, "Survey over image thresholding techniques and quantitative performance evaluation", *Journal of Electronic Imaging*, **13(1)**, 146-165, January 2004

[3] A. M. Gambaruto, J. Peiró, D. J. Doorly, A. G. Radaelli, "Reconstruction of shape and its effect on flow in arterial conduits", *Int. J. Numer. Meth. Fluids*, 2008; **57**(5):473–692.

[4] J. Kittler and J. Illingworth, "Minimum Error Thresholding", *Pattern recognition*, Vol **19**, No 1, pp 41–47, 1986

[5] Nobuyuki Otsu, "A Threshold Selection Method from Gray-Level Histograms", *IEEE Transactions on Systems, Man and Cybernetics*, vol **SMC-9**, No 1, January 1979

[6] T. W. Ridler and S. Calvard, "Picture Thresholding Using an Iterative Selection Method", *IEEE Transactions on Systems, Man and Cybernetics*, vol **SMC-8**, No 8, August 1978

[7] Pietro Perona and Jitendra Malik, "Scale-Space and Edge Detection Using Anisotropic Diffusion", *IEEE Transactions on Pattern Analysis and Machine Intelligence*, Vol **12**, No 7, July 1990

[8] Greg Turk and James F. O'Brien, "Shape Transformation Using Variational Implicit Functions", *Proc. of the ACM SIGGRAPH*, pp. 335-342, August 1999, Los Angeles

[9] Ireneusz Tobor, Patrik Reuter and Christophe Schlick, "Efficient Reconstruction of Large Scattered Geometric Datasets using Partition of Unity and Radial Basis Functions", *Research Report RR-1301-03*, University of Bordeaux, 2003

[10] Jules Bloomenthal, "An Implicit Surface Polygonizer", *Academic Press Graphics Gems Series*, **Graphics Gems IV**, pp 324-349, 1994

# Assessment of the viscous/molecular subgrid-scale dissipation terms in LES based on transport equations

Sara Rego, Carlos B. da Silva, and José C. F. Pereira

*IDMEC/IST, Mecânica I, 1º andar/LASEF,*
*Av. Rovisco Pais, 1049-001 Lisbon,*
*PORTUGAL.*

*sararego@sapo.pt*

## Abstract

One trend in large-eddy simulations (LES) involves the use of a transport equation for the subgrid-scale (SGS) kinetic energy. For problems involving active or passive scalar fields a SGS scalar variance transport equation is also used. The terms from these equations involve sub-filter scale quantities that are not accessible during LES and thus require modelling. By far the greatest challenge for modelling in these equations comes from the *viscous and the molecular SGS dissipation* terms that represent the final (dissipation) stages of the "energy cascade mechanism" whereby the SGS kinetic energy and SGS scalar variance are dissipated through the action of the molecular viscosity and diffusivity, respectively. In this work direct numerical simulations (DNS) of statistically stationary (forced) homogeneous, isotropic turbulence are used to (*i*) analyse the topology and spatial localisation of the viscous and the molecular SGS dissipation terms, (*ii*) assess three models currently used for these terms and, (*iii*) present some guidelines to improve or develop future models for these terms. The models analysed here are (*a*) the classical model [1, 2], (*b*) the model used in hybrid RANS/LES [3, 4], and (*c*) the model for the molecular SGS dissipation of SGS scalar variance from Jiménez *et al.* [5]. The analysis uses correlation coefficients, joint probability density functions (PDFs), several one point statistics such as the variance, skewness, and the flatness factors, as well as spectra from the exact and modelled molecular SGS dissipations. Results show that the classical models for the molecular SGS dissipation give very good results in terms of their topology, spatial localisation (in the physical space), statistical behaviour, and spectral characteristics. Moreover, the model constants approach asymptotically the theoretical values as the Reynolds number and filter sizes increases, which supports the use of a constant value in engineering and geophysical applications, instead of using a dynamic procedure for their computation as in reference [6]. For the molecular SGS dissipation of SGS scalar

variance the model from Jiménez *et al.* [5] performs even better than the classical model and should be the preferred model for this term when the Schmidt number is close to 1.0. Finally, all the tests showed that the models used in hybrid RANS/LES tested here give very poor results either in terms of its topological, statistical or spectral characteristics. The reason behind this is connected with the deficient spectral representation of the exact molecular SGS dissipation term. More details are given in [7]

**Keywords:** Subgrid-scale modelling, Viscous/molecular SGS dissipation, Isotropic turbulence, Direct Numerical Simulations.

# References

[1] U. Schumann. Subgrid-scale model for finite difference simulations of turbulent flows on plane channels and annuli. *J. Comp. Phys.*, 18:376–404, 1975.

[2] A. Yoshizawa. A statistically-derived subgrid model for the large-eddy simulation of turbulence. *Phys. Fluids*, 25(9):1532–1538, 1982.

[3] E. G. Paterson and L. J. Peltier. Detached-eddy simulation of high-reynolds-number beveled-trailling-edge boundary layers and wakes. *J. Fluids Eng.*, 127:897–906, 2005.

[4] K. Hanjalic. Will RANS survive LES? a view of perspectives. *J. Fluids Eng.*, 127:831–839, 2005.

[5] C. Jiménez, F. Ducros, B. Cuenot, and B. Bédat. Subgrid scale variance and dissipation of a scalar field in large eddy simulations. *Phys. Fluids*, 13(6):1748–1754, 2001.

[6] S. Ghosal, T. Lund, P. Moin, and K. Akselvol. A dynamic localisation model for large-eddy simulation of turbulent flows. *J. Fluid Mech.*, 286:229–255, 1995.

[7] C. B. da Silva, Sara Rego, and J. C. F. Pereira. Analysis of the viscous/molecular subgrid-scale dissipation terms in les based on transport equations: A priori tests. *Journal of Turbulence*, (in Press), 2008.

# Intense vorticity structures topology near the rotacional/irrotacional interface in plane jets

Ricardo José Nunes dos Reis
Carlos Bettencourt da Silva
José Carlos Fernandes Pereira
*LASEF, IST, Portugal.*
*rreis@aero.ist.utl.pt http://www.lasef.ist.utl.pt*

## Abstract

All shear layer flows (like boundary layers, mixing layers, wakes and jets) have two diferent regions: a high enstrophy region and an irrotacional region. Separating the two an interface can be define, through which irrotacional fluid chunks gain vorticity and are absorved into the turbulent flow. The mechanism responsible for this governs the rate of mass, momentum, temperature, etc, transfers from the irrotacional to the rotacional flow and, as such, is of primordial interest [2].

Contrary to the accepted theory since the 60/70s, it has been proven, in the last decade, that the physical process governning this transfers is related to small scale activity (nibling) (see [1]). Meanwhile the presence of intense vorticity structures near the interface indicate that the last is shaped by them and they account for important effects to it's phenomenology (see fig. (2)) .

The topology of intense vorticity structures (ISV) is characterized near the rotacional/irrotacional interface of plane jets has in [4],[3] for isotropic turbulence. The results were obtained from a plane jet Direct Numerical Simulation. The radius, length and vorticity of these structures is in average bigger in the plane jet than in isotropic turbulence (see figs. (3), (4) and (5)). These parameters were also characterized in relation to their distance to the interface, has their preferred orientation related to the interface tangent (see fig. (6))

**Keywords:** turbulence, rotacional/irrotacional interface, plane jet, intense vorticity structures

# References

[1] David K. Bisset, Julian C. R. Hunt, and Michale M. Rogers. The turbulent/non-turbulent interface bounding a far wake. *J. Fluid Mech.*, 451:383–410, 2002.

[2] Carlos B. da Silva and José C. F. Pereira. Invariants of the velocity-gradient, rate-of-strain, and rate-of-rotation tensors across the turbulent/nonturbulent interface in jets. *Physics of Fluids*, 20(5):055101, 2008.

[3] J. Jiménez and A. Wray. On the characteristics of vortex filaments in isotropic turbulence. *J. Fluid Mech.*, 373:255–285, 1998.

[4] J. Jimenez, A. Wray, P. Saffman, and R. Rogallo. The structure of intense vorticity in isotropic turbulence. *J. Fluid Mech.*, 255:65–90, 1993.
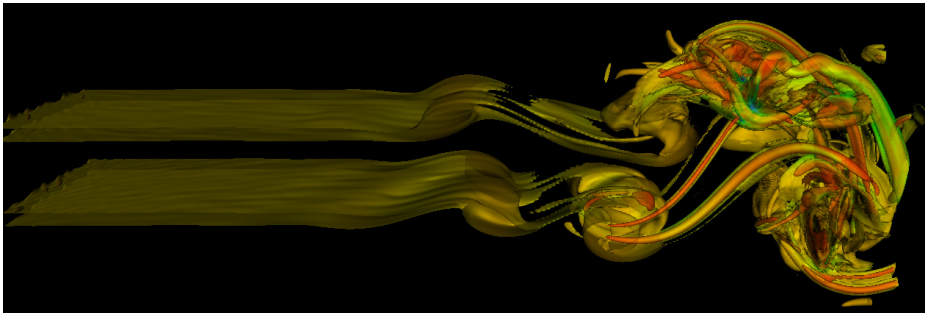
Figure 1: Plane jet, side view, vorticity contours
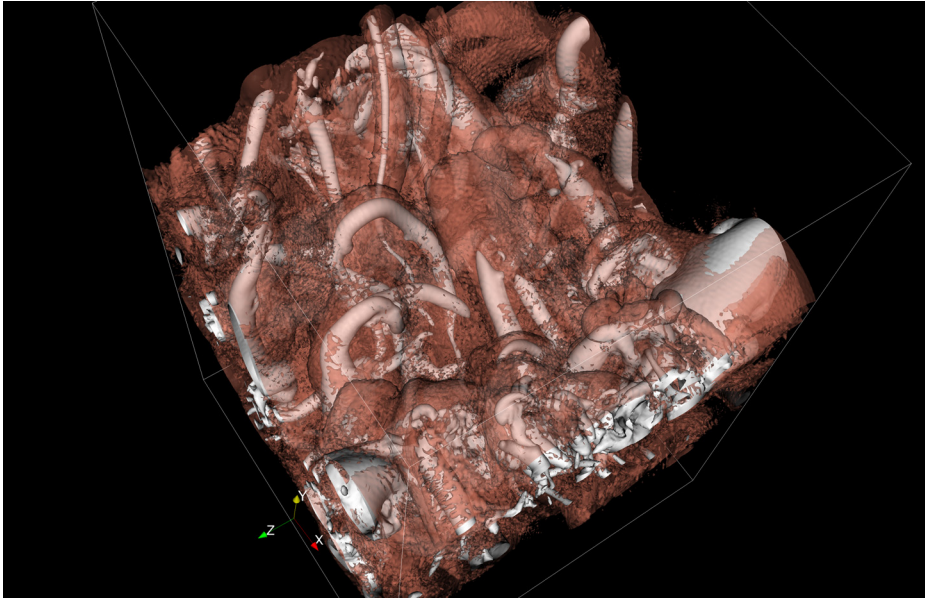
Figure 2: Interface and ISVs
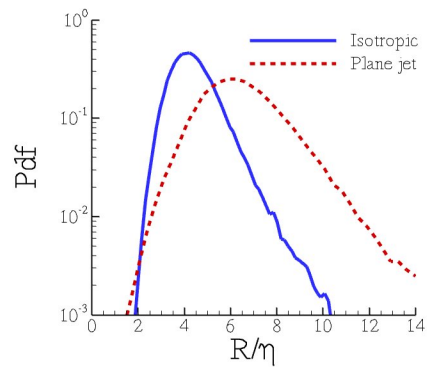


Figure 3: ISV $R/\eta$
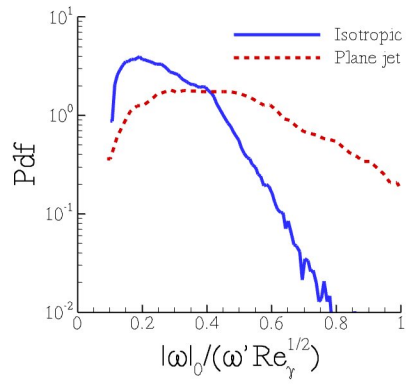
Figure 4: ISV $\omega_0/(\omega' Re^{\frac{1}{2}})$
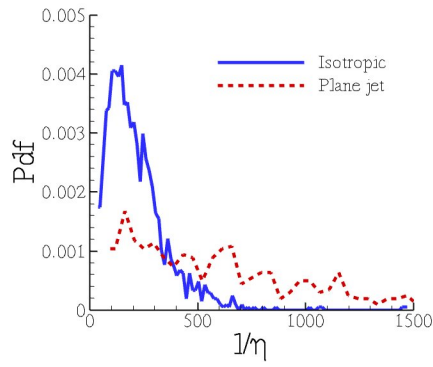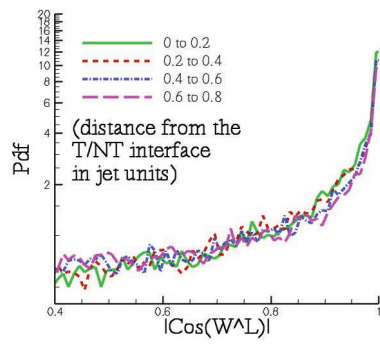


Figure 5: $length/\eta$ of ISVs

Figure 6: ABS(cos) of angle of vorticity and interface surface tangent

# Cell nucleus GFP flow analysis from sequences of LSCFM images

Isabel Rodrigues[1,2] and João Sanches[2]

[1]*Instituto Superior de Engenharia de Lisboa*
*, [2]Systems and Robotic Institute / Instituto Superior Técnico*
*Lisbon, Portugal*

[†] E-mail: *João Sanches: jmrs@ist.utl.pt*

*Laser Scanning Fluorescence Confocal Microscopy* (LSFCM) is nowadays one of the most important tools in biomedicine research. In fact, it makes possible to accurately study the dynamic processes occurring inside the cell and its nucleus by following the motion of fluorescent molecules along the time. Due to the small amount of acquired radiation and the huge optical and electronics amplification, the LSFCM images are usually corrupted by a severe type of Poisson noise. This noise may be even more damaging when very low intensity incident radiation is used to avoid *phototoxicity* during long time acquisition processes.

In this paper a Bayesian algorithm is proposed to remove the Poisson *multiplicative* noise corrupting the LSFCM images. The observations are organized in a 3D tensor where each plane is one of the images acquired along the time of a cell nucleus using the *Fluorescence Loss In Photobleaching* (FLIP) technique. The method removes the noise by considering simultaneously different spatial and temporal correlations. This is done by using an anisotropic 3D filter that may be separately tunned in space and time dimensions. Tests using real data are described and presented to illustrate the application of the algorithm.

## 1    Introduction

The answer to the question *'How do living cells function?'* has been a matter of intensive study all over the years. For a long time biologists have had their work based on dehydrated and chemically fixed specimen, to guess what processes could be found in living cells and how they were supposed to occur.

The fortunate combination of the use of fluorescent proteins with the invention of the confocal microscope in 1988 by M. Minsky, triggered an important change in the course of the biomedical research.

Fluorescence was already known for quite a long time. It was on 1852 when Stokes reported it for the first time, referring to the now well known, Green Fluorescent Protein (GFP) *Aequorea Victoria*. The GFP's can be incorporated into a cell as protein marker by a process of fusion with the gene encoding the protein of interest, followed by a stable or transient transfection into the cell. This way, tagged proteins can be visualized in living cells in an almost non-invasive manner, without the need for prior fixation.

When a photon of energy $E = \hbar c/\lambda$ ($\lambda$ is the photon wavelengths in vacuum) is absorbed by the fluorophore all its energy is transferred to the fluorescent molecule, forcing it into an excited state. The return to the fundamental state can be accomplished by the emission of a photon with a larger wavelength. This particular manner of disposing energy gives rise to the phenomenon of fluorescence.

When another photon is absorbed, the fluorophore, with high probability, will go through *forbidden transitions* to attain very unstable states and consequently showing high predisposition towards photochemical reactions with the surrounding molecules, causing irreversible destruction of the fluorescence. This phenomenon is called the *photobleaching effect*. This is in general an undesirable effect. Since all the fluophores will eventually photobleach upon extended excitation, the image acquisition becomes more and more diffi-

cult as time goes by. Due to the small amount of detected radiation and the huge optical and electronics amplification, the LSFCM images exhibit a severe type of noise Poisson noise, typical of low photon count processes.

Nevertheless, some techniques such as Fluorescence Recovery After Photobleaching (FRAP) and Fluorescence Loss In Photobleaching (FLIP), take advantage of this not always sole damaging effect to study some dynamic processes occurring inside the cells [1].

The Confocal Microscope was invented in 1988 by M. Minsky. It consisted of two lenses located in each side of the specimen (the illumination objective and the detection objective) and two pinholes, one in front of the illumination and the other in front of the detection. The ensemble shows an elegant symmetry, as can be seen in scheme of Fig. 1.
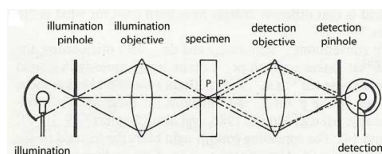


Figure 1: Sceme of M. Minsky Confocal Microscope.

The name *Confocal* comes from the fact that the illumination and the detection objectives form an image of their respective pinholes onto the same spot. The great novelty of this system is that the pinhole prevents the light emanating from the out-of-focus points from reaching the detector, which gives the microscope the capability to illuminate a thin plane of the specimen to be observed.

The Florescence Confocal Microscope presents a slight difference from the previous one. The wavelength of the incident light is shorter then the one emitted by the fluorescent proteins. The fluorescence emission is separated from the excitation by a beam splitter and an emission filter.

The Laser Scanning Fluorescence Confocal Microscope (LSFCM) is basically a Fluorescence Confocal Microscope with a coupled scanning device to allow the acquisition of 2-D images.

Due to the advances in the LSFCM [2], to the development of synthetic probes and proteins and improvements in the production of a wider spectrum of laser light sources coupled to highly accurate acoustic/optic controlled filters, the fluorescence confocal microscopy has became one of the most powerful tools in medical and biological research [3].

In human cells, after being released from th transcription sites which are distributed throughout the nucleoplasm, messenger ribonucleoproteins (mRNP) must reach the nuclear pore complexes (NPC) in order to be translocated to the cytoplasm. The aim of this work is to study the nature of this transport, whence quantitative Photobleaching methods were developed in order to investigate the mobility of mRNP's within the nucleus of the human living cells.

Photobleaching techniques such as FLIP are employed to selectively destroy fluorescent molecules within a region of interest (ROI) with a high intensity laser, followed by monitoring the recovery of new fluorescent molecules into the bleached area, over a period of time with a low intensity laser. The resulting information can then be used to determine the kinetic properties, including diffusion coefficients, mobile fraction and transport rate of the fluorescently labeled molecules.

In a FLIP experiment, a selected region in the cell expressing fluorescently tagged proteins is illuminated with repetitive bleach pulses of a high intensity focused laser beam within the ROI and imaged between

pulses. The fluorescence loss is then measured in a region further away from the bleached area. The rate of fluorescence recovery is related to the mobility of the molecules inside the cell and can be the result of diffusion processes, chemical reactions and associations or transport processes [2].

For the FLIP experiment in the present work, RNP complexes were made fluorescent by transient expression of GFP fused to two distinct mRNA- binding proteins: PABPN1 and TAP. The HeLa cell was used.

Cells were repeatedly bleached at intervals of $3.64s$ and imaged between pulses. Bleaching was performed by $279ms$ bleach pulses on a spot of $1.065\mu m$ radius (30 pixels diameter). A series of 350 images $512 \times 512$ pixels was collected for each studied cell.

In this work a denoising algorithm is proposed for LSFCM images where the FLIP technique is used.

The denoising algorithm is formulated in the Bayesian framework where a Poisson distribution models the observation noise and a Gibbs distribution, with *log-Total variation* and *log-quadratic* potential functions, regularizes the solution, defining the field to be estimated as a *Markov Random Field* (MRF). These potential functions have shown to be more appropriated to deal with this type of optimization problems in $R_+^N$ [4]. The regularization is performed in the image space and in time (time courses) using different priors and different prior parameters. The denoising iterative algorithm involves an anisotropic 3D filtering process to cope with the different smoothing effects performed in the space and time dimensions.

Tests using real data are presented to illustrate the application of the algorithm. In the next section the problem is formulated from a mathematical point of view.

## 2 Model

The sequence under analysis, $\mathbf{Y}$, is the result of a FLIP experiment. Data can be represented by a 3D tensor, $\mathbf{Y} = \{y(i,j,t)\}$, containing a stack of $L$ *laser scanning fluorescence confocal microscopy* (LSFCM) images with $0 \leq i, j, t \leq N-1, M-1, L-1$. Each image at the discrete time $t_0$, $y(i,j,t_0)$, is corrupted by Poisson noise as well as each time course associated with the pixel $(i_0, j_0)$, $y(i_0, j_0, t)$. In this paper the image sequences correspond to $L$ observations of HeLa nucleus in FLIP experiments as described above. The goal of this study is to estimate the underlying cell nucleus morphology, $\mathbf{X}$, from the noisy observed images, $\mathbf{Y}$, exhibiting a very low *signal to noise ratio* (SNR).

A Bayesian approach is adopted to estimate $\mathbf{X}$ by solving the following optimization problem

$$\hat{\mathbf{X}} = \arg\min_{\mathbf{X}} E(\mathbf{X}, \mathbf{Y}) \tag{1}$$

where the energy function is a sum of two terms, $E(\mathbf{X}, \mathbf{Y}) = E_Y(\mathbf{X}, \mathbf{Y}) + E_X(\mathbf{X})$. $E_Y(\mathbf{X}, \mathbf{Y})$ is called the *data fidelity term* and $E_X(\mathbf{X})$ is called the *prior term*. The first term pushes the solution toward the observations according to the type of noise corrupting the images and the prior term smooths the solution [5, 6]. Under the assumption of independence of the observations, the *data fidelity term* is defined as

$$E_Y(\mathbf{X}, \mathbf{Y}) = -\log\left[\prod_{i,j,t} p(y(i,j,t)|x(i,j,t))\right]. \tag{2}$$

Since the images are corrupted by Poisson noise, $p(y|x) = \frac{x^y}{y!}e^{-x}$, the log data fidelity term is

$$E_Y(\mathbf{X}, \mathbf{Y}) = \sum_{i,j,t} x(i,j,t) - y(i,j,t)\log(x(i,j,t)) + C \tag{3}$$

where $C$ is a constant term .

Here an anisotropic prior term is used, in the sense that the penalization between neighboring pixels is one value for pixels at the same image (spatial correlation) and another for neighboring pixels from different images (time course correlation). Both priors in space and in time are Gibbs distributions with *log-Euclidean* potential functions in time (to smooth the time courses) and *log-Total variation* potential functions in space (to preserve edges). These log potential functions are the more appropriated when the unknowns to be estimated are all positive [4, 7],

$$p(\mathbf{X}) = \frac{1}{Z} e^{-U(\mathbf{X})} \tag{4}$$

where

$$U(X) = \alpha \sqrt{\log^2\left(\frac{x(i,j,t)}{x(i-1,j,t)}\right) + \log^2\left(\frac{x(i,j,t)}{x(i,j-1,t)}\right)} + \beta \log^2\left(\frac{x(i,j,t)}{x(i,j,t-1)}\right) \tag{5}$$

The prior term is $-\log E_X(\mathbf{X})$ and therefore the overall energy function to be minimized is

$$
\begin{aligned}
E(\mathbf{X}, \mathbf{Y}) \quad = \quad & \sum_{i,j,t} [x(i,j,t) - y(i,j,t)\log(x(i,j,t))] \\
+ \quad & \alpha \sum_{i,j,t} \sqrt{\log^2\left(\frac{x(i,j,t)}{x(i-1,j,t)}\right) + \log^2\left(\frac{x(i,j,t)}{x(i,j-1,t)}\right)} \\
+ \quad & \beta \sum_{i,j,t} \log^2\left(\frac{x(i,j,t)}{x(i,j,t-1)}\right)
\end{aligned}
\tag{6}
$$

The minimization of this energy function (6) is not a convex problem and its optimization using *gradient descendent* or Newton-Raphson based methods is difficult. However, performing an appropriate change of variable $z(i,j,t) = H(x(i,j,t))$, it is possible to turn it into convex. Let $z(i,j,t) = H(x(i,j,t)) = \log(x(i,j,t))$ or $x(i,j,t) = e^{z(i,j,t)}$. The function $H(x)$ is monotonic and therefore the minimizers of $E(\mathbf{X}, \mathbf{Y})$ and $E(\mathbf{Z}, \mathbf{Y})$ are related by $\mathbf{Z}^* = \log(\mathbf{X}^*)$. The new energy function becomes

$$
\begin{aligned}
E(\mathbf{Z}, \mathbf{Y}) \quad = \quad & \sum_{i,j,t} \left[ e^{z(i,j,t)} - y(i,j,t)z(i,j,t) \right] \\
+ \quad & \alpha \sum_{i,j,t} \sqrt{(z(i,j,t) - z(i-1,j,t))^2 + (z(i,j,t) - z(i,j-1,t))^2} \\
+ \quad & \beta \sum_{i,j,t} (z(i,j,t) - z(i,j,t-1))^2
\end{aligned}
\tag{7}
$$

where $\alpha$ and $\beta$ are prior parameters to tune the level of smoothing across the images and across the time courses respectively.

The minimization of (7) is performed by finding its stationary point according to the first order condition

$$\nabla E(\mathbf{Z}, \mathbf{Y}) = 0 \tag{8}$$

To solve this huge optimization problem we use a Newton's algorithm and reweighted least squares based method where the weights are updated in each iteration and are obtained by using a specific MM algorithm

proposed in [5, 8]. The approximate solution to this problem is then computed by iteratively calculating:

$$z(i,j,t)^{(k+1)} = z(i,j,t)^{(k)} - \frac{F(z(i,j,t)^{(k)}}{W(z(i,j,t)^{(k)}} \tag{9}$$

where $k$ stands for the iteration number and

$$
\begin{aligned}
F\left(z(i,j,t)\right) = \;& e^{z(i,j,t)} - y(i,j,t) + \left[\alpha\left(2w + w_a + w_c\right) + 4\beta\right]z(i,j,t) \\
& - \alpha\left[w\left(z(i-1,j,t) - z(i,j-1,t)\right) + w_a\left(z(i+1,j,t)\right) + w_c\left(z(i,j+1,t)\right)\right] \\
& - 2\beta\left(z(i,j,t-1) - z(i,j,t+1)\right)
\end{aligned}
\tag{10}
$$

where

$$w = \frac{1}{\sqrt{\left(z(i,j,t) - z(i-1,j,t)\right)^2 + \left(z(i,j,t) - z(i,j-1,t)\right)^2}} \tag{11}$$

$$w_a = \frac{1}{\sqrt{\left(z(i+1,j,t) - z(i,j,t)\right)^2 + \left(z(i+1,j,t) - z(i,j-1,t)\right)^2}} \tag{12}$$

$$w_c = \frac{1}{\sqrt{\left(z(i,j+1,t) - z(i-1,j+1,t)\right)^2 + \left(z(i,j+1,t) - z(i,j,t)\right)^2}} \tag{13}$$

$$W(i,j,t) = e^{z(i,j,t)} + \alpha\left(2w + w_a + w_c\right) + 4\beta \tag{14}$$

Reversing the change of variable, the final solution is

$$\hat{\mathbf{X}} = e^{\mathbf{Z}} \tag{15}$$

# 3    Experimental results

The sequences of real data under analysis, $\mathbf{Y}$, are the results of FLIP experiments as described above. The 3D tensor $\mathbf{Y} = \{y(i,j,t)\}$ represents the stack of *laser scanning fluorescence confocal microscopy* (LSFCM) images where no background was subtracted. The only preprocessing performed on the acquired data was a simple alignment procedure to correct for cell nucleus displacement during image acquisition, that consisted of a set of rigid body transforms driven by the maximization of the correlation between images.

In order to estimate $\mathbf{X}$, the aligned images were then processed using the denoising methodology described above. The CPU time of the algorithm was 1.2$s$ *per* iteration in a Centrino Duo 2.00GHz, 1.99 GB RAM processor. The results for three images of each stack are shown in Figs. 2, 3 and 4 where each row represents a time instant. The first column stands for the raw data, the second column shows the results for the described denoising algorithm and in the third column results for a similar denoising algorithm using a log-Euclidean prior in space (instead of log-Total variation) are presented for comparison. As can be seen in these figures there is a great deal of improvement in the quality of the representation when using the presented algorithm. The blurr present in the denoised images in the third column results from the *log-quadratic* prior used to remove the noise. This undesirable effect is attenuated by using the log-Total variation prior which is edge preserving.
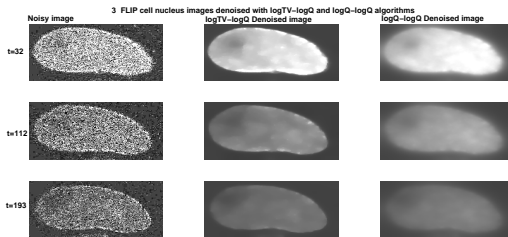
Figure 2: Raw data and filtered data of HeLa immortal cell nucleus for t=32, 112, 193.
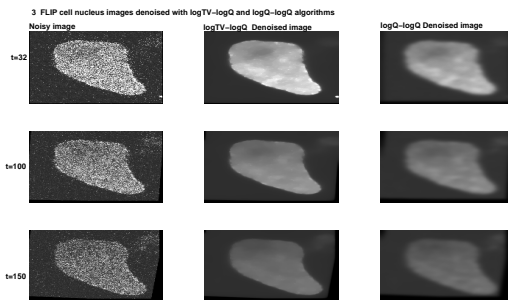


Figure 3: Raw data and filtered data of HeLa immortal cell nucleus for t=32, 100, 150.

Improvements can also be noticed in the time dimension. Results for two time courses of one of the nucleus are shown in Fig. 5. Both plots show noisy and denoised time courses outside (left) and inside (right) the bleached region.

A graph-cuts segmentation procedure was performed on the denoised data in order to display the propagation of the fluorescence loss that occurs inside the nucleus with time. The segmentation results for instants $t = 10, 75$ of the denoised images of one of the cells nucleus are shown in Fig. 6 (a) and (c); results for the companion segmentation can be see in Fig. 6 (b) and (d). As shown in the figure, the fluorescence loss spreads inside the nucleus from a region around the bleached area toward the edges of the nucleus, particularly on the left side, since the bleach area is not standing in the center of the nucleus.

## 4 Conclusions

In this paper a new denoising algorithm is proposed to *Laser Scanning Fluorescence Confocal Microscopy* (LSFCM) imaging with *photobleaching*. The sequence of LSFCM images taken along the time, in this microscopy modality, are corrupted by a type of multiplicative noise described by a Poisson distribution.
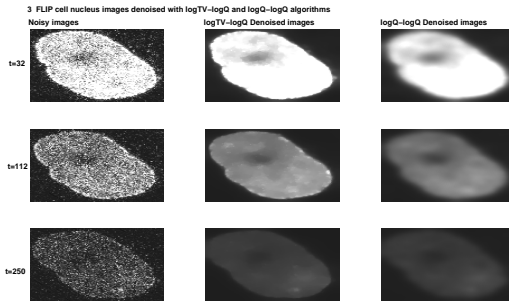
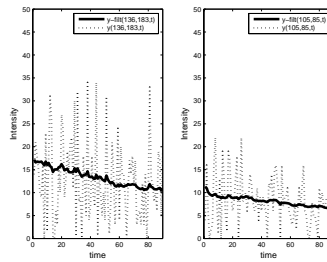Figure 4: Raw data and filtered data of HeLa immortal cell nucleus for t=32, 112, 250.



Figure 5: Time courses outside the bleach region (a) and inside the bleached region (b).

Furthermore, the global intensity of the images decreases along the time due to permanent fluorophore loss of its ability to fluoresce, caused by chemical reactions induced by the incident laser and by other surrounding molecules. The decreasing on the image intensity is "associated" to a decreasing on the signal to noise ratio of the images, making the biological information recovery a difficult task [9].

In this paper a Bayesian algorithm is proposed to perform a simultaneous denoising procedure in the space (images) and in time (time course) dimensions. This approach, conceived as an optimization task with the *maximum a posteriori* (MAP) criterion, leads to a filtering formulation involving a 3D (2D+time) anisotropic filtering procedure. The energy function is designed to be convex and its minimizer is computed by using the Newton's algorithm and a reweighted least squares based method which allows continuous convergence toward the global minimum, in a small number of iterations.

Tests using real data have shown the ability of the methodology to reduce the multiplicative noise corrupting the images and the time courses.
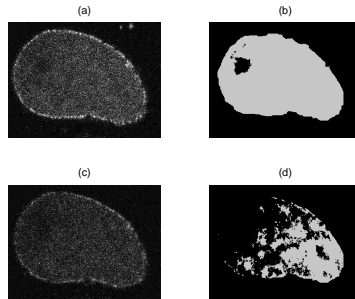
Figure 6: Photobleaching propagation across the nucleus from the bleached area. Raw data (left) and segmentation results (right) for images $t = 10$ and $t = 75$.

# Acknowledgment

# References

[1] J. Lippincott-Schwartz, N. Altan-Bonnet, and G. H. Patterson, "Photobleaching and photoactivation: following protein dynamics in living cells." *Nat Cell Biol*, vol. Suppl, September 2003. [Online]. Available: http://view.ncbi.nlm.nih.gov/pubmed/14562845

[2] R. Underwood, "Frap and flip, photobleaching technique to reveal cell dynamics," 2007. [Online]. Available: http://www.nikoninstruments.com/images/stories/litpdfs/ nikon_note_3nn06_8_07_lr.pdf

[3] J. W. Lichtman and J. A. Conchello, "Fluorescence microscopy." *Nat Methods*, vol. 2, no. 12, pp. 910–9, 2005.

[4] V. Arsigny, P. Fillard, X. Pennec, and N. Ayache, "Log-Euclidean metrics for fast and simple calculus on diffusion tensors," *Magnetic Resonance in Medicine*, vol. 56, no. 2, pp. 411–421, August 2006.

[5] T. K. Moon and W. C. Stirling, *Mathematical methods and algorithms for signal processing.* Prentice-Hall, 2000.

[6] J. M. Sanches and J. S. Marques, "Joint image registration and volume reconstruction for 3d ultrasound," *Pattern Recogn. Lett.*, vol. 24, no. 4-5, pp. 791–800, 2003.

[7] S. Boyd and L. Vandenberghe, *Convex Optimization.* Cambridge University Press, March 2004.

[8] N. J., S. J.M., and M. J.S., "An unified framework for bayesian denoising for several medical and biological imaging modalities," in *Proceedings IEEE EMBC 2007.* Lyon, France: IEEE International Conference of the Engineering in Medicine and Biology Society (EMBS), August 23-26 2007.

[9] N. A. M. A. Lashin, "Restoration methods for biomedical images in confocal microscopy," Ph.D. dissertation, Berlin, 2005.

# 2D Boundary Element Method (BEM) for non-Newtonian fluid flows

Sellountos J. Euripides

*CEMAT, IST Technical University of Lisbon, Portugal.*
*esell@math.ist.utl.pt*

Adélia Sequeira

*CEMAT, IST Technical University of Lisbon, Portugal.*
*adelia.sequeira@math.ist.utl.pt*

## Abstract

The Boundary Element Method (BEM) is presented for the solution of the generalized Navier - Stokes equations. The velocity - vorticity formulation is adopted, where the kinematics and kinetics aspects are seperated from the pressure computation. In the present formulation no derivatives are involved in the coupling between the kinematics and kinetics. The convective parabolic - diffusion fundamental solution is used resulting on a very effective upwind scheme for the transport equation. The results are compared with FEM solutions and show good agreement.
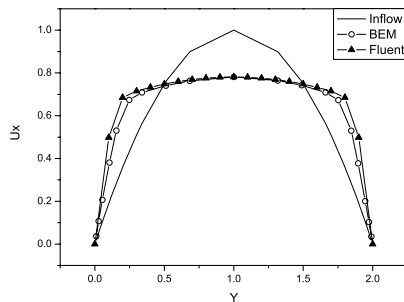
**Keywords:** Boundary Element Method (BEM), velocity-vorticity, non-Newtonian flow.
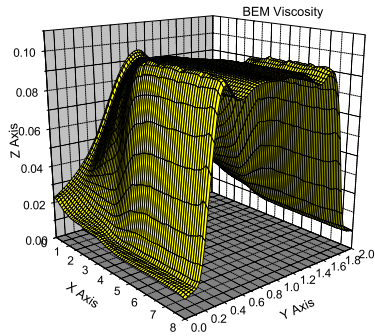
# References

[1] L. Skerget, N. Samec, *BEM for non-Newtonian fluid flow*, Engineering analysis with Boundary Elements, 23, (1999) 435-442.

[2] Skerget L, Hribersek M, Zunic Z (2003) *Natural convection flows in complex cavities by BEM*, Int J Numer Meth Heat Fluid Vol:13(5/6) 720–736.

[3] Sellountos EJ, Sequeira A, *An advanced meshless LBIE/RBF method for solving two dimensional incompressible fluid flows*, Computational Mechanics, Vol. 41, No. 5, pp. 617-631, 2008 (DOI: 10.1007/s00466-007-0219-1.Published Online: Oct 2007).

[4] Sellountos EJ, Sequeira A, *A hybrid multi-region BEM / LBIE-RBF velocity-vorticity scheme for the two-dimensional Navier-Stokes equations*, CMES Computer Modeling in Engineering and Sciences, Vol. 23, No.2, pp. 127-148, 2008 (Published Online in 2007).

# Characterizing the flow field using critical point theory with relation to typical atherosclerosis location

Gonçalo Silva

*Departamento de Engenharia Mecânica, Instituto Superior Técnico, Portugal.*
*goncalo.silva@ist.utl.pt*

Francesca Anselmi

*Dipartimento di Ingegneria dell'Informazione, Università degli Studi di Padova, Italia.*
*francesca.anselmi@gmail.com*

Alberto M. Gambaruto

*CEMAT,Departamento de Matemática, Instituto Superior Técnico, Portugal.*
*alberto.gambaruto@yahoo.com*

Adélia Sequeira

*CEMAT,Departamento de Matemática, Instituto Superior Técnico, Portugal.*
*adelia.sequeira@math.ist.utl.pt*

## Abstract

The use of critical point theory in fluid mechanics has arisen from a necessity to interpret and analysing complex fluid flow patterns, and well adapted for the study of high resolution data of from CFD [1]. The present work applies critical point theory to the computational study of fluid dynamics where atherosclerosis diseases typical occur. Three different geometries are used and shown in Figure 1; two are idealisations of physiological geometries, namely an elbow and a stenosis, while the third geometry is a peripheral bypass graft obtained from *in vivo* MRI. The stenosis of the simplified geometry has the same characteristics as the stenosis in the peripheral bypass graft geometry. The flow structures are characterized using critical point theory and are relate to the typical occurrence locations of atherosclerosis.

The flow is modelled as Newtonian, steady, incompressible and laminar, and the computations are performed using Fluent. Segmentation and reconstruction methods used for the bypass graft geometry are described in [2] and the same geometry as $G_u^{100}$ is used in their work for our simulations.
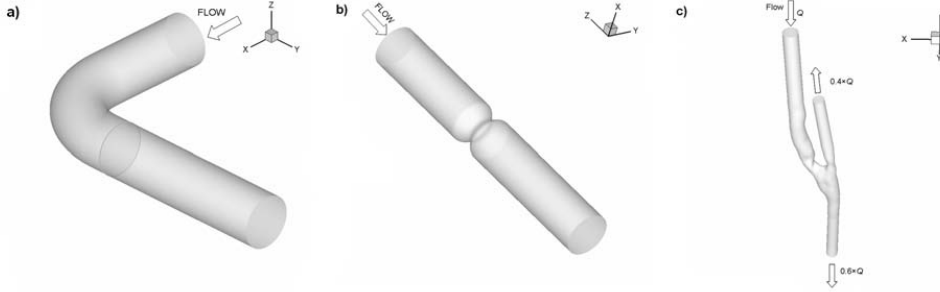
Figure 1: Surface boundaries of considered for numerical simulations: a) elbow geometry; b) stenosis geometry; c) peripheral bypass graft geometry

A critical point is defined as the location in the flow field where the streamline slope is indeterminate and at least two of the velocity components $u_i$ are zero relative to an appropriate observer, hence

$$\frac{u_i}{u_j} = \frac{0}{0} \quad , \text{ where } i \neq j \tag{1}$$

According to [3], if the velocity field $u_i(x_j, t)$ of a uniform-density and incompressible flow is known, then an arbitrary point P can be chosen so that it is possible to expand, using a Taylor series, the velocity $u_i$ in terms of the space coordinates $x_j$, where the origin of $x_j$ is located at P. It follows that:

$$u_i(x_j, t) = A_i + A_{ij}x_j + A_{ijk}x_jx_k + A_{ijkl}x_jx_kx_l + \dots. \tag{2}$$

From the critical point definition, if P is a critical point then the zeroth order term $A_i, i = 1, 2, 3$, is zero. Therefore, the topological features describing the flow field are given by the properties of the first non zero term in the Taylor series expansion and are valid in the vicinity of the critical points.

Critical points can be divided into two different types: free-slip critical points, which are characterized by the properties of the first order derivative term in Equation (2); and no-slip critical points, which are characterized by the properties of the second order derivative term. An example of a no-slip critical point is a separation point on a no-slip boundary. The identification and characterization of the flow structures are given by the eigenvalues of the derivative terms of Equation (2). As described in [4], the presence of complex eigenvalues indicates a vortical structure; while the exclusive presence of real eigenvalues indicates a saddle and/or a node structure.
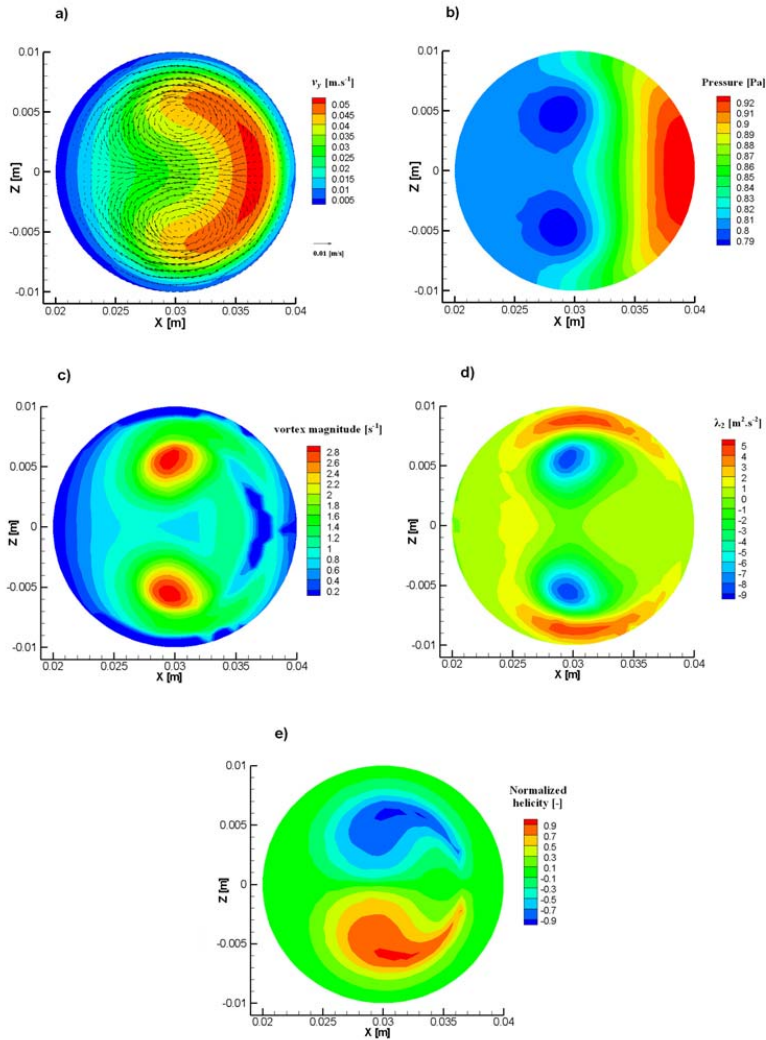
Figure 2: Contour plots of the elbow geometry cross-section as indicated in Figure 1. a) Velocity field; b) pressure field; c) magnitude of complex eigenvalue from critical point theory; d) magnitude of $\lambda_2$; e) normalized helicity

Following the work of [5],[6], as well as substantial supporting literature, we observe the regions of the flow with low wall shear stress (WSS) to be correlated to preferential sites of atherosclerosis formation. We note that for the elbow geometry, atherosclerosis occurs preferentially along the inner wall of the bend, and for the stenosis geometry it occurs preferentially in the region of slow recirculation downstream of the stenosis. In the case of the bypass graft geometry the regions at risk are considered to be the toe, heel and floor of the anastomosis.

Vortical structures identified using critical point theory are compared to those provided by two other methods: the $\lambda_2$ criterion [7] and normalized helicity [8]. The results obtained for the elbow geometry, shown in Figure 2, reveal good agreement of the Dean vortices between the different approaches, acknowledging the use of critical point theory to characterize flow structures.

Critical point theory furthermore yields a greater insight into the behaviour of the flow field which other methods do not provide. This is firstly due to the fact that critical point theory can also identify node/saddle structures in the flow field. Secondly, the eigenvectures of the derivative terms can give information on the principal axes of the vortical structure or node/saddle configurations. Thirdly the eigenvalues of the derivative terms yield the relative spacing of the streamlines around a critical point as well as identify the direction of the streamlines, hence if the vertical structure or node/saddle configurations are stable or unstable.

**Keywords:** Critical point theory, flow field characterisation, CFD, flow structures, flow patterns linked to atherosclerosis.

# References

[1] A. E. Perry, M. S. Chong. "A description of eddying motions and flow patterns using critical-point concepts"' *Ann. Rev. Fluid Mech.*, 1987; 19: 125–155.

[2] Gambaruto A.M., Peiró J., Doorly D.J., Radaelli A.G. "Reconstruction of Shape and its Effect on Flow in Arterial Conduits"' *International Journal for Numerical Methods in Fluids*,2008;**(57)**(5):473–692.

[3] A. E. Perry, M. S. Chong. "A series-expansion of the Navier-Stokes equation with applications to three-dimensional separation patterns" *Ann. Rev. Fluid Mech.*, 1986; 173:207–223.

[4] M. S. Chong, A. E. Perry, B. J. Cantwell. "A general classification of three-dimensional flow fields" *Phys. Fluids A*, 1990; **(2)**(5):765–777.

[5] D.M. Wootton, D.N. Ku. "Fluid Mechanics of Vascular Systems, Diseases, and Thrombosis" *Annu. Rev. Biomed. Eng.*, 1990; 01:299–329.

[6] S. Giordana, S. J. Sherdwin, J. Peiró, D. J. Doorly, J. S. Crane, K. E. Lee, N. J. W. Cheshire, C. G. Caro "Local and global geometric influence on steady flow in distal anastomoses of peripheral bypass grafts" *Journal of Biomechanical Engineering*, 2005; 127:1087–1098.

[7] J. Jeong, F. Hussain. " On the identification of a vortex" *J. Fluid Mech.*, 1995; 285:69–94.

[8] Y. Levy, D. Degani, A. Seginer. "Graphical visualization of vortical flows by means of helicity" *AIAA J.*,1990;**(28)**(8):1347–1352.

# Numerical simulations of three-dimensional effects in "infinite" swept wing tests at supersonic flow conditions

J. M. M. Sousa

*IDMEC/IST, Mecânica I, 1º andar/LASEF,*
*Av. Rovisco Pais, 1049-001 Lisbon,*
*PORTUGAL.*
*msousa@ist.utl.pt*

## Abstract

Skin friction drag on an aircraft wing has a significant impact on specific fuel consumption, pollution and noise emissions. In the EU-funded project SUPERTRAC (SUPERsonic TRAnsition Control), various concepts are explored to achieve viscous drag reduction on supersonic aircraft wings (Arnal *et al.*, 2006). The problem has been widely studied for both subsonic and transonic flows but information on the feasibility of laminar flow control techniques at supersonic speeds is still scarce. Two-dimensional Euler simulations have been used to design "infinite" swept wing models with the aim of testing the concepts in a wind tunnel. It was found that good agreement with experiments occurs in cases characterized by a supersonic leading-edge, *i.e.* for low sweep angles or a conjunction of high Mach number and high sweep angle. However, it was also found that significant discrepancies occur for a subsonic leading-edge. This observation triggered the need for additional numerical simulations with the objective of clarifying the role of viscous effects and the validity of the "infinite" swept wing approach.

# References

[1] . Arnal, C.G. Unckel, J. Krier, J.M.M. Sousa and S. Hein (2006) Supersonic laminar flow control studies in the SUPERTRAC project, *25th Congress of the International Council of the Aeronautical Sciences*, ICAS 2006, September 3-8, Hamburg, Germany.